

Colossal Magnetoresistance

N. Shirato

Course: Solid State Physics 2, Spring 2010, Instructor: Dr. Elbio Dagotto
 Department of Materials Science and Engineering, University of Tennessee, Knoxville, TN 37996 and
 (04/08/2010)

Colossal magnetoresistance (CMR) effect was discovered among the manganese oxide class of materials, i.e. $\text{La}_{1-x}\text{Ca}_x\text{MnO}_3$. It shows large magnetoresistance by orders of magnitude, however several environmental requirements limit CMR toward general applications. Recently people have been focused on understanding a fundamental physics because of complex correlations between electron-lattice and electron-electron interactions, which gives rise to a rich variety of physical phenomena. Basic theories which have been published to explain CMR are introduced in the paper.

Introduction

From the classical electrodynamics, magnetoresistance (MR), which was first discovered by W. Thomson in 1856, is the material property to change its electrical conductivity when a presence of an external magnetic field. Although normally a change of the conductivity is in an order of few percentage, there has been several technologies crucially used in our life, which are based on the MR. The discovery of the giant magnetoresistance (GMR) in the late 1980's has another enormous influence into our life[4, 5]. Thinly layered magnetic and non-magnetic materials were found that they exhibit increase or decrease of their resistivity by more than 20 percent under relatively weak external magnetic fields. This GMR opened new electronics where the electron spin plays a key role in the operation of electronic devices. Few years later of GMR discovery, the materials were found that could exhibit the change of an electric resistance not by a few percent but by orders of magnitude, hence this phenomenon was named the colossal magnetoresistance (CMR). The CMR is generally found in doped manganite perovskites such as $\text{RE}_{1-x}\text{M}_x\text{MnO}_3$ (RE = rare earth, M = Sr, Ca, Ba)[7].

The CMR effect can be extremely large resulting in a resistance change of a few orders in magnitude. CMR originates from a metal-insulator transition in the low temperature near the Curie temperature (TC) the vicinity of TC and requires magnetic fields of the order of several Tesla.

In the technological applications view points, we can make the MR factor very close to 100%, however this occurs unfortunately at the cost of reducing TC. GMR presents MR changes with as small as 0.01 T, while CMR typically needs larger fields of about 1 T or more for equivalent resistivity changes. This seems too large for potential use in magnetic recording devices. Hence, the manganites will be mainly considered as an interesting basic-physics problem[7]. CMR materials are interesting from a fundamental viewpoint. In contrast to traditional ferromagnets such as Fe, Co and Ni where the spin system is isolated from the lattice, in the manganites the charge, spin, and lattice degrees of freedom are strongly coupled together, which are strongly correlated electron systems, leading to a delicate balance of interactions that gives rise to a rich variety of physical phenomena of current interest in condensed matter science [3, 9].

Quantitatively Schiffer et al. exhibits CMR phenomena at $x = 1/4$ of $\text{La}_{1-x}\text{Ca}_x\text{MnO}_3$. The Fig. 1 shows the magnetization and resistivity as a function of temperature, and the existence of a robust MR, larger than 80%. The drop in resistivity with decreasing temperature and the peak in MR are correlated with the ferromagnetic transition in the magnetization. At this concentration, the insulating behavior above TC is very prominent, on the other hand below TC ferromagnetism is present[7]. The Fig. 2 is phase diagram of $\text{La}_{1-x}\text{Ca}_x\text{MnO}_3$ from experimental measurements. There are several different phases, which are mixture of ferromagnetic/antiferromagnetic and metal/insulator phases. The interpretation and understanding the mechanism of these different phases are crucial.

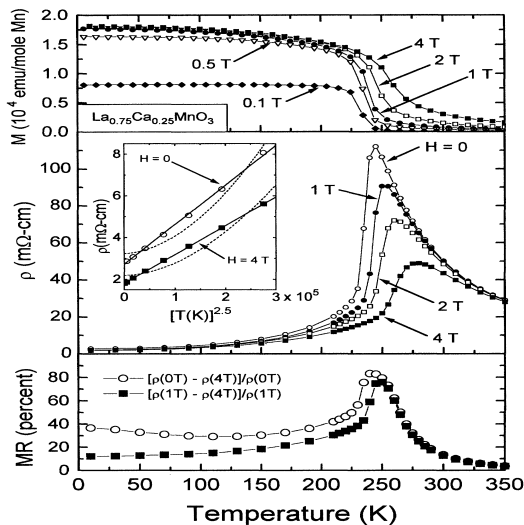


Figure 1: The magnetization, resistivity, and magnetoresistance of $\text{La}_{0.75}\text{Ca}_{0.25}\text{MnO}_3$ as a function of temperature at various field. The inset shows ρ at low temperatures. [12]

The physical features of CMR manganites

Crystal structure:

The structure of the $\text{La}_{1-x}\text{Ca}_x\text{MnO}_3$ oxides is close to that of the cubic perovskite. The crystal structure and lattice parameters can be obtained by neutron powder diffraction [11].

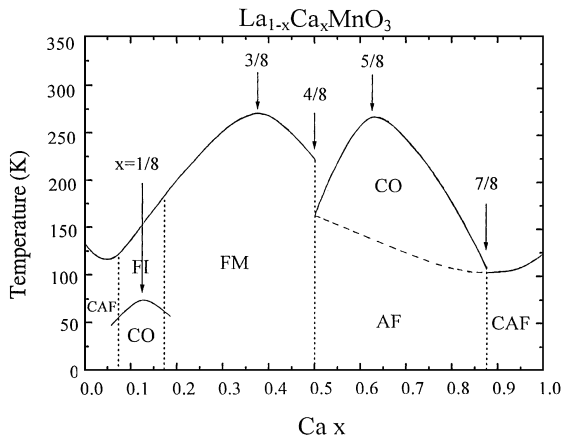


Figure 2: Phase diagram of $\text{La}_{1-x}\text{Ca}_x\text{MnO}_3$, constructed from measurements of macroscopic quantities such as the resistivity and magnetic susceptibility. [6] FM: Ferromagnetic Metal, FI: Ferromagnetic Insulator, AF: Antiferromagnetism, CAF: Canted Antiferromagnetism, and CO: Charge/Orbital Ordering.

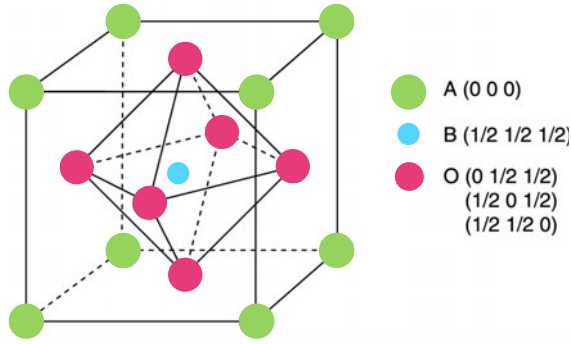


Figure 3: The cubic perovskite of $\text{La}_{1-x}\text{Ca}_x\text{MnO}_3$ manganites. The large sized Lanthanum (trivalent rare earth) ions occupy the A-site with 12-fold oxygen coordination. The smaller Mn ions in the mixed-valence state Mn^{3+} OR Mn^{4+} are located at the centre of an oxygen octahedron, the B-site with 6-fold coordination. [3]

The large sized Lanthanum (trivalent rare earth) ions and Calcium (divalent alkaline earth) ions occupy the A-site with 12-fold oxygen coordination [3]. The smaller Manganese ions in the mixed-valence state $\text{Mn}^{3+}-\text{Mn}^{4+}$ are located at the center of an oxygen octahedron, the B-site with 6-fold coordination. For the stoichiometric oxide, the proportions of Mn ions in the valence states 3+ and 4+ are respectively, $1-x$ and x . For instance, LaMnO_3 is isostructural, crystallizing in the orthorhombic $Pnma$ structure at the ambient condition. The octahedra are elongated and tilted, and it's believed the result of a Jahn-Teller local distortion (Fig. 4) [11].

Electric properties:

For an isolated 3d ion, generally five degenerated orbital states are available to the 3d electrons. In a crystal, the degen-

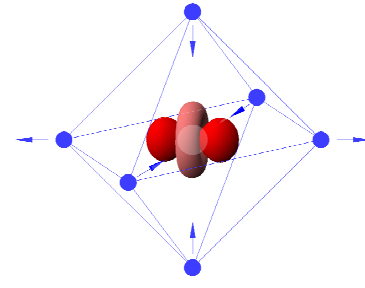


Figure 4: The Jahn-Teller distortion on a cubic perovskite. The distortion of oxygen octahedron causing splitting of Mn d orbitals. $3y^2 - r^2$ orbital caused by the degeneracy can be observed. [1]

eracy is partly lifted by the crystal field. In the cubic lattice environment, due to the Jahn-Teller (JT) distortion the five-fold degenerate 3d-orbitals of an isolated atom or ion are split into a manifold of three lower energy levels (d_{xy} , d_{yz} , and d_{zx}), usually referred to as t_{2g} once mixing with the surrounding oxygen is included, and two higher energy states ($d_{x^2-y^2}$ and $d_{3z^2-r^2}$) called e_g [7, 11].

For the MnO_6 octahedron, the splitting between the lowest t_{2g} level and the highest e_g level is $\Delta \sim 1.5$ eV [3, 11]. We consider the valence of the Mn-ions is either four (Mn^{3+}) or three (Mn^{4+}), and their relative fraction is controlled through chemical doping (proportions of Mn ions in 3+ and 4+ are $1-x$ and x respectively)[3]. The Hund coupling exchange energy of about 2.5 eV being larger than the crystal field splitting, Mn^{3+} is $3d^4$, $t_{2g}^3 e_g^1$ with $S = 2$ whereas Mn^{4+} is $3d^3$, t_{2g}^3 with $S = \frac{3}{2}$. Hence, the large Hund coupling favors the population of the t_{2g} levels with three electrons forming a spin $S=3/2$ state, and the e_g level either contains one electron or none [3].

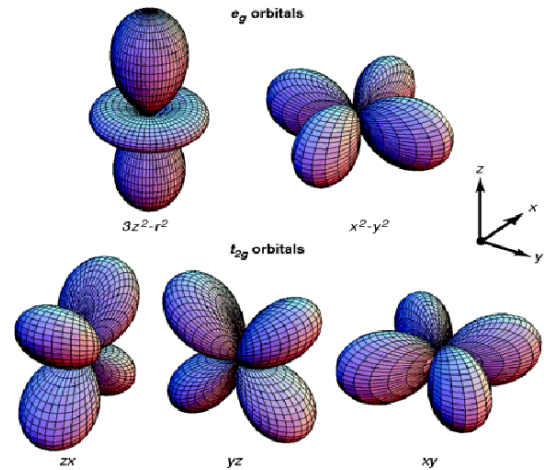


Figure 5: Five different types of d orbitals degeneracy caused by cubic lattice and JT distortion. [2]

The large value of the electron-phonon coupling is clear in the regime of manganites below $x = 1/5$ where a static JT distortion plays a key role in the physics of the material. In a crystal field of symmetry lower than cubic, JT distortion produces important fluctuations that localize electrons by splitting the degenerate e_g levels at a given MnO_6 octahedron. In

the detail, if the spins order along the z-axis, then the LS interaction λLS immediately stabilizes the orbitals with the z component of the angular momentum $L_z = \pm 1$ or $L_z = \pm 2$ instead of $L_z = 0$ [3]. Depending on the sign of λ , the orbitals are chosen so that L_z and the spin align in a parallel or antiparallel way. In the octahedron surroundings of the ligand atoms,

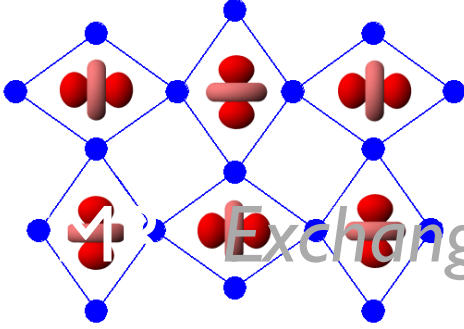


Figure 6: J-T distortion and orbital ordering on ab plane. [1]

a JT distortion occurs in such a way that the octahedron elongates in the z direction because the electrons occupy nonzero L_z states, such as yz and zx orbitals. This is characterized as the coupling between the orbital ordering and JT distortion (Fig. 6) [9].

Besides, although the energy of Mn^{4+} remains unchanged by JT distortion, the energy of Mn^{3+} is lowered (Fig. 7). Thus, Mn^{3+} has a preferred tendency to distort its octahedral environment compared to Mn^{4+} . This would explain that JT distortion is rather effective in the lightly doped manganites (large concentration of Mn^{3+}); the JT distortions are not independent from one Mn^{3+} site [3, 9]. This is illustrated in Fig. 6 by the structure of $LaMnO_3$ in which the MnO_6 octahedra are strongly elongated within the ab plane. By increasing the Mn^{4+} content, the JT distortions are reduced and the stabilization of the $3z^2 - r^2$ e_g orbital becomes less effective. Nevertheless, in a large number of manganites, the e_g orbitals of two types, $3z^2 - r^2$ and $x^2 - y^2$ are not occupied by the e_g electrons of Mn^{3+} at random and an orbital order is achieved [3].

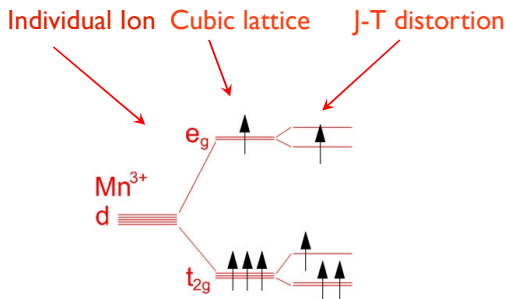


Figure 7: Energy level diagram of the degenerated Mn^{3+} ions 3d orbital by the cubic lattice and JT distortion. [1]

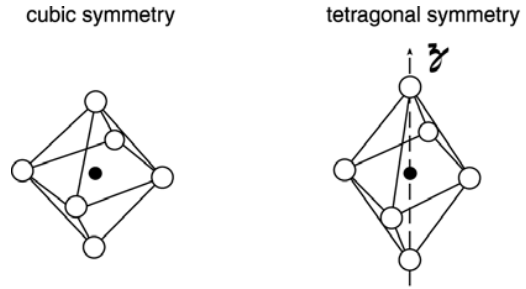


Figure 8: A crystal field of cubic and tetragonal symmetry of Mn^{3+} ions. [3]

Theory of magnetic and metallic phases

Super Exchange and Double Exchange interactions:

Origin of the magnetic properties of the manganites are governed by exchange interactions between the Mn ion spins. These interactions are relatively large between two Mn spins separated by an oxygen atom and are controlled by the overlap between the Mn d-orbitals and the O p-orbitals [3, 7]. The corresponding “super exchange interactions” depend on the orbital configuration. Generally, for $Mn^{4+}-O-Mn^{4+}$, the interaction is AF, whereas for $Mn^{3+}-O-Mn^{3+}$ it may be FM or AF (Fig. 9), such as in $LaMnO_3$ where both F and AF interactions coexist [1, 7, 10]. The detail mechanism of the super exchange interaction is described in the following charge ordering section.

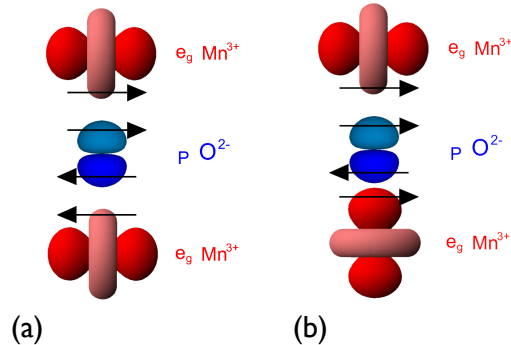


Figure 9: Super exchange interactions between $Mn^{3+}-O^{2-}-Mn^{3+}$. The interactions depend on orbital configuration. (a) This configuration exhibits “anti-ferromagnetic” type interaction. (b) This configuration exhibits “ferromagnetic” type interaction. [1]

An interesting case is that of $Mn^{3+}-O-Mn^{4+}$, for which the Mn ions can exchange their valence by a simultaneous jump of the e_g electron of Mn^{3+} on the Oxygen p-orbital and from the Oxygen p-orbital to the empty e_g orbital of Mn^{4+} . This mechanism of “double exchange interactions” (DE) originally proposed by Zener in 1951 [13] explains a strong ferromagnetic-type interaction [3]. The DE correlates strongly with the Hund coupling, which is explained in the following section. In this process there are two simultaneous motions involving spin up

electron moving from the oxygen to the right Mn-ion, and another spin up electron from the left Mn-ion to the oxygen (Fig. 10) [7].

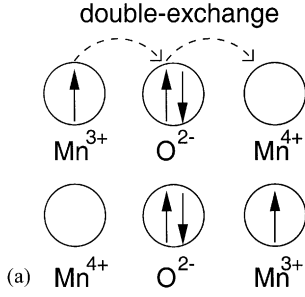


Figure 10: Sketch of the Double Exchange (DE) mechanism which involves two Mn ions and O ion. [7]

The Hund coupling:

The Hund coupling is an electron-electron interaction causing by same electron spin directions and angular momentum. In the case of Mn^{3+} , the e_g and t_{2g} electrons interact through the Hund coupling. In this situation, when the e_g electrons directly jump from Mn to Mn their kinetic energy is minimized if all spins are aligned. This procedure to obtain ferromagnetism is usually also called double-exchange (DE) [3, 7, 9, 11].

Charge ordering:

A periodic pattern of filled and empty sites is said to exhibit charge ordering. For manganites, Goodenough [8] theoretically explained the AFM phase at $x=1/2$ of $\text{La}_{1-x}\text{Ca}_x\text{MnO}_3$ [7]. At $x=1/2$, a real-space ordering of charge carriers takes place when their long-range Coulomb interaction overcomes the kinetic energy [3]. This huge nearest-neighbor Coulomb repulsion can stabilize the system. Hence, from the theory it was assumed that the charge was distributed in a checkerboard pattern, upon which spin and orbital order was found (Fig. 11) [7, 11].

In the detail of Goodenough's theory, we consider a Mn-O bond directed along the z-axis, and let us assume that the Mn-cation has an occupied orbital pointing along x or y instead of z (in other words, there is an empty orbital along z) in Fig. 9 (a). Because the oxygen ion does not have a negative cloud of Mn electrons, the oxygen in O^{2-} state, will try to move towards the top Mn^{2+} site. This process shortens the distance Mn-O and makes a stable bond [7]. Suppose now the occupied Mn-orbital has an electron with an up (right) spin. Of the two relevant electrons of oxygen, the one with spin up (right) will feel the exchange force toward the Mn electron [If both electrons involved have the same spin, the space part of their common wave function has nodes which reduce the electron-electron repulsion (as in the Hund's rules)] [7, 9]. Then, effectively the considered Mn-O bond becomes ferromagnetic between the Mn electron and one of the oxygen electrons.

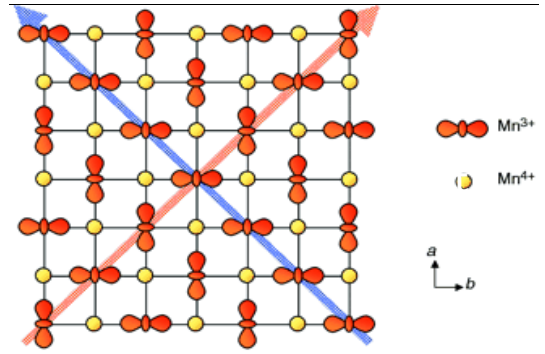


Figure 11: When $x=1/2$ of $\text{La}_{1-x}\text{Ca}_x\text{MnO}_3$. The charge ordering of Mn^{3+} and Mn^{4+} ions are shown along the ab plane. [2]

Now consider the bottom of O-Mn portion of the Mn-O-Mn bond in Fig. 9 (a). In the example under consideration, the second electron of oxygen must be down (left) and it stays away from the top Mn^{2+} . If the Mn^{2+} on the bottom of the link Mn-O-Mn also has an occupied orbital pointing perpendicular to the z-axis, then O-Mn and Mn-O behave similarly (individually FM) but with pairs of spins pointing in opposite directions. As a consequence an effective antiferromagnetic Mn-Mn interaction has been generated (Fig. 9 (a)), and both Mn-O and O-Mn are shortened in length [7, 11]. However, if the bottom Mn^{2+} has an orbital pointing along z (along the relevant p-orbital of the oxygen), the Hund-rule-like argument does not apply anymore (direct exchange), leading to an AF O-Mn bond (Fig. 9 (b)) [7]. In this case, the overall Mn-Mn interaction is ferromagnetic. Then, simple arguments lead to the notion that both AF and FM couplings among the Mn-ions can be effectively generated, depending on the orientation of the orbitals involved [3, 7, 9, 11].

Orbital ordering:

Orbital-ordering gives rise to the anisotropy of the electron-transfer interaction. This favors or disfavors the double-exchange interaction or the super exchange interaction in an orbital direction-dependent manner. Hence gives a complex spin-orbital coupled state. Besides, as explained in the previous section the orbital-ordering is coupled with the Jahn-Teller distortion (Fig. 6) [3, 9].

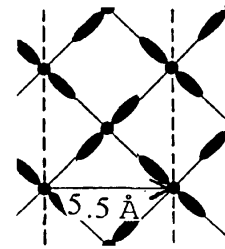


Figure 12: When $x=0$ of $\text{La}_{1-x}\text{Ca}_x\text{MnO}_3$. The orbital ordering of Mn^{3+} ions, which is strongly correlated with JT distortions, can be observed. [6]

Spin ordering:

Interactions with neighboring atoms make the spin of electrons align in a particular fashion. Ferromagnetism occurs when the spins are arranged parallel to one another. Antiferromagnetism results when they are anti-parallel to one another. There are particularly three types of antiferromagnetic ordering in perovskite-type oxides (Fig. 13) [3, 7, 9, 11].

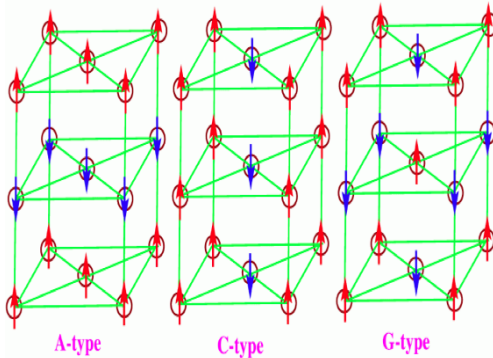


Figure 13: Three different types of antiferromagnetic order in 3D perovskite structure. A-type: The intra-plane coupling is ferromagnetic while inter-plane coupling is antiferromagnetic. C-type: The intra-plane coupling is antiferromagnetic while inter-plane coupling is ferromagnetic. G-type: Both intra-plane and inter-plane coupling are antiferromagnetic. [2]

Interpretation of the phase diagram of $\text{La}_{1-x}\text{Ca}_x\text{MnO}_3$

The explanation of the physical properties of $\text{La}_{1-x}\text{Ca}_x\text{MnO}_3$ is crucial. Due to the compound has rich and complex phases and magnetic properties, people have been worked to understand the change of properties with the theories, which are listed in previous sections.

$$x = 0:$$

When the zero chemical doping, whereas LaMnO_3 is found to be an AF insulator from the phase diagram in Fig. 2 with a gap in the half-filled e_g band resulting from the JT distortion. In this system, only Mn^{3+} ions are located on the lattice, hence as explained in the previous section, Mn^{3+} ions are orbitally ordered with strongly correlating JT distortion. Besides from Fig. 11, one can see ferromagnetic type orbital ordering in 2D from the super exchange configuration (Fig. 9 (b)), however in 3D, there are anti-ferromagnetic configurations between each layer, which is A-type AF (Fig. 13).

$$x = 1/3:$$

A half-metallic ferromagnetic ground state is obtained at $x = 1/3$, with the electronic structure near the Fermi level mainly

consisting of substantially hybridized bands derived from majority spin Mn e_g states and O p states. The transfer of e_g electron from Mn^{3+} to Mn^{4+} by DE is the basic mechanism of electrical conduction in the manganites. In those with strong DE, the e_g electrons become delocalized in the ferromagnetic phase for a certain range of doping centred around $x = 1/3$ and a FM state is established at low temperature [3]. This would explain in Fig. 2 at high temperature the compound shows insulator type feature, but as the temperature gets lowered the compound starts exhibiting metallic type ferromagnetism.

$$x = 1/2:$$

The well-known CE-type AFM [7]. From Fig. 11 the configuration exhibits charge/orbital/spin ordering. This CE-type arrangement is quite stable among all kinds of doping concentration. In the phase diagram, it's shown at the boundary between F and AF phases (Fig. 2).

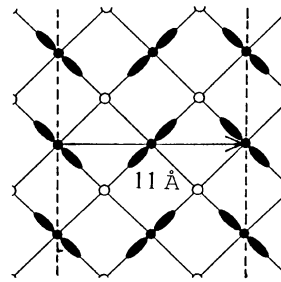


Figure 14: Mn^{3+} and Mn^{4+} ions arrangement at $x=1/2$. The black symbol is Mn^{3+} and the white empty dot is Mn^{4+} . [6]

$$x = 2/3:$$

When increasing x above $1/2$, the number of ferromagnetic DE links decreases and that of AF coupled Mn^{4+} increases [3]. This favors AF or canted AF phases in which the motion of charge carriers is hindered [7, 11]. In the phase diagram, at high temperature it's insulator and as the temperature decreases CO (Charge/Orbital ordered) and AF phases appears respectively (Fig. 2).

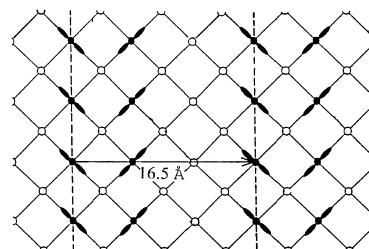


Figure 15: Mn^{3+} and Mn^{4+} ions arrangement at $x=2/3$. Bi-stripe type AF arrangement. The black symbol is Mn^{3+} and the white empty dot is Mn^{4+} . [6]

$$x = 1:$$

At this concentration, only Mn^{4+} are located on the lattice. Similar to $x = 0$, as the temperature gets lowered the phase gets changed to insulator to AF metal (Fig. 2). Specifically, this AF has G-type AF as shown in Fig. 13 [7, 9, 11].

Conclusion

Since the discovery of CMR manganites, it has attracted huge attentions. Specifically this 3d transition-metal oxides, possess large magnetoresistivity, which easily exceeds GMR, at relatively low temperature. This large magnetoresistivity in these oxides is the result of a unique type of metal–insulator transition. These oxides have a rich and complex physics related to the large importance of electron–lattice and electron–electron interactions. Their structural, magnetic and

transport properties are intricately related. For that, it is necessary to understand a fundamental physics behinds the phenomenon. Exchange interactions, the Hund coupling and charge/orbital/spin orderings have been used to explain physical properties of CMR manganites, however there are still numerous unknown phenomena, which can't be explained by the theories. Numerical, computational simulations have been heavily applied for solving the complex phenomenon, and people would expect these methods will be crucial to answer the questions.

References

- [1]http://solidstate.physics.sunysb.edu/talk/2006_bme_web/
 [2]<http://folk.uio.no/ravi/activity/ordering/colossal-magnet.html>
-
- [1] magnetoresistant materials: the key role of phase separation. *Physics Reports*, 344(1-3):1 – 153, 2001.
 [2] J.B. Goodenough. *Phys. Rev.*, 100:564, 1955.
 [3] J-P Renard A-M Haghiri-Gosnet. Cmr manganites: physics, thin films and devices. *Journal of Physics D: Applied Physics*, 36(8):R127, 2003.
 [4] M. N. Baibich, J. M. Broto, A. Fert, F. Nguyen Van Dau, F. Petroff, P. Etienne, G. Creuzet, A. Friederich, and J. Chazelas. Giant magnetoresistance of (001)fe/(001)cr magnetic superlattices. *Phys. Rev. Lett.*, 61(21):2472–2475, Nov 1988.
 [5] G. Binasch, P. Grünberg, F. Saurenbach, and W. Zinn. Enhanced magnetoresistance in layered magnetic structures with antiferromagnetic interlayer exchange. *Phys. Rev. B*, 39(7):4828–4830, Mar 1989.
 [6] Hwang H.Y. Cheong, S.W. *Contribution to Colossal Magnetoresistance Oxides, Monographs in Condensed Matter Science*. Gordon Breach, London, 1999.
 [7] Elbio Dagotto, Takashi Hotta, and Adriana Moreo. Colossal magnetoresistant materials: the key role of phase separation. *Physics Reports*, 344(1-3):1 – 153, 2001.
 [8] J.B. Goodenough. *Phys. Rev.*, 100:564, 1955.
 [9] Masatoshi Imada, Atsushi Fujimori, and Yoshinori Tokura. Metal-insulator transitions. *Reviews of Modern Physics*, 70(4), 10 1998/10/1/.
 [10] Shraiman B.I. Littlewood-P.B. Millis, A. *Phys. Rev. Lett.*, 74:5144, 1995.
 [11] A P Ramirez. Colossal magnetoresistance. *Journal of Physics: Condensed Matter*, 9(39):8171–8199, 1997.
 [12] P. Schiffer, A. P. Ramirez, W. Bao, and S-W. Cheong. Low temperature magnetoresistance and the magnetic phase diagram of $\text{La}_{1-x}\text{Ca}_x\text{MnO}_3$. *Physical Review Letters*, 75(18), 10 1995/10/30/.
 [13] C. Zener. *Phys. Rev.*, 82:403, 1951.